Low-Cost Plasmonic Platform for Photon-Emission Engineering of Two-Dimensional Semiconductors

Anuj Kumar Singh,[1] Kishor K. Mandal,[1] Yashika Gupta,[1] Abhay Anand V.S.,[1] Lekshmi Eswaramoorthy,[1] Brijesh Kumar,[1] Abhinav Kala,[2] Saurabh Dixit,[1] Venu Gopal Achanta,[2,*] and Anshuman Kumar[1,†]

[1] *Department of Physics, Laboratory of Optics of Quantum Materials, IIT Bombay, Mumbai 400076, India*

[2] *Department of Condensed Matter Physics and Material Science, Tata Institute of Fundamental Research, Homi Bhabha Road, Mumbai 400005, India*

(Received 10 July 2022; revised 14 December 2022; accepted 23 February 2023; published 5 April 2023)

Although the field of two-dimensional (2D) materials has democratized materials science by making high-quality samples accessible cheaply, due to the atomically thin nature of these systems, an integration with nanostructures is almost always required to obtain a significant optical response. Traditionally, these nanostructures are fabricated via electron beam lithography or focused ion beam milling, which are expensive, and large-area fabrication can be further time-consuming. In order to overcome this problem, we report the integration of 2D semiconductors on a cost-effective and large-area fabricated nanocone platform. We show that the plasmon modes of our nanocone structures lead to photoluminescence enhancement of monolayer WSe_2 by about eight to ten times compared with the nonplasmonic case, consistent with finite-difference time-domain simulations. Excitation power-dependent measurements reveal that our nanocone platform enables a versatile route to engineering the relative exciton trion contributions to the emission.

DOI: 10.1103/PhysRevApplied.19.044012

I. INTRODUCTION

Monolayers of transition-metal dichalcogenides (TMDCs) are optically active direct-band-gap semiconductors [1–4] which have been shown to be promising candidates for optoelectronic applications [5,6] such as sensing [7], photovoltaics [8], and quantum information [9,10]. The integration of these two-dimensional (2D) semiconductor TMDCs with nanostructures can not only strengthen the light-matter interaction [11,12] but also help engineer their optical response for various applications [13–16]. Although the field of 2D materials has democratized materials science [17] by making high-quality samples accessible cheaply, due to the atomically thin nature of these systems, an integration with nanostructures is almost always required to obtain a significant optical response [12]. Traditionally, these nanostructures are fabricated via electron beam lithography or focused ion beam milling, which are expensive, and large-area fabrication can be further time-consuming [18]. In order to overcome this problem, we report the integration of 2D semiconductors on a cost-effective and large-area fabricated nanocone platform. We fabricate polytetrafluoroethylene (PTFE) nanocone structures and decorate it with a gold (Au) film, enabling it to behave like a plasmonic antenna array. We show that the plasmon modes of our nanocone structures lead to photoluminescence (PL) enhancement of monolayer WSe_2 by about eight to ten times compared to the nonplasmonic case. PL enhancement is further verified via finite-difference time-domain (FDTD) simulations. Excitation power-dependent as well as the time-dependent measurements reveal that our nanocone platform enables a versatile route to engineering the relative exciton trion contributions to the emission.

II. METHODS

A. Fabrication of nanocone array

Large-scale fabrication of nanocones was carried out via a colloidal lithography approach [19,20]. First, PTFE substrates, purchased from Sigma Aldrich (GF46787259-1EA) were cleaned using ethanol for 5 min in an ultrasonicator and then washed with deionized water. Next, the substrates were treated with an oxygen plasma for 2 min to make them hydrophilic. Polystyrene (PS) microbeads were deposited on this modified PTFE surface using convective self-assembly [21,22].

The process flow diagram for the fabrication of the cone array is shown in Fig. 1(a), where two glass slides

*achanta@tifr.res.in
†anshuman.kumar@iitb.ac.in

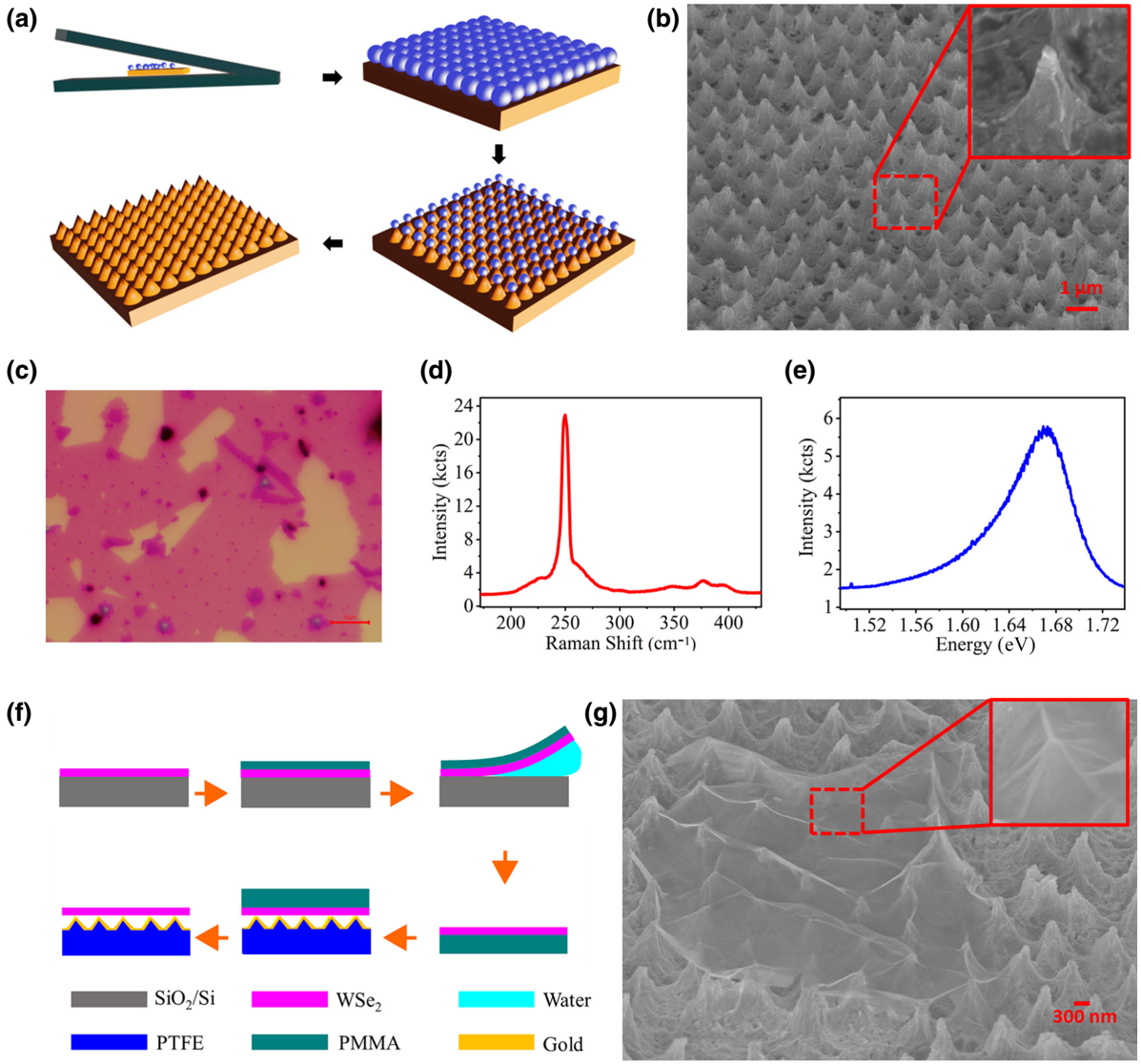

FIG. 1. Fabrication of the TMDC integrated plasmonic nanocone structures. (a) Process flow diagram for the fabrication of PTFE cone array. (b) SEM image of large-scale PTFE nanocone array after etching (inset showing an enlarged view of the cone). (c) Optical microscopy image of the large-area CVD-grown WSe_2 monolayer. (d) Raman spectrum confirming the monolayer. (e) PL spectra of the monolayer WSe_2. (f) Process flow diagram for the wet transfer method. (g) SEM image of the WSe_2 monolayer transferred over the cone array (inset showing the WSe_2 over single cone).

were aligned to form 1° wedge angle for the deposition of the PS microparticles and a diluted 1% suspension of PS microparticle was then injected into the wedge. This assembly was carefully kept undisturbed for 2 h, allowing the suspension liquid to evaporate, leaving behind a PS microbead monolayer covering the substrate. The surface of the monolayer of PS microparticles was then exposed to an oxygen plasma to reduce the size of the deposited PS microparticles and, in turn, etch out the exposed PTFE film below to form nanocones with the etching time. This etching was carried out via reactive ion etching in an oxygen plasma maintained at 0.2 mbar pressure and 40 sccm gas flow rate with 100 W rf power. The etching parameters were optimized to obtain an array of PTFE nanocones surmounted by residues of PS microparticles. These residues were removed by rinsing the sample in ethanol.

Figure 1(b) shows the post-etching scanning electron microscopy (SEM) image of the as-fabricated PTFE cone array on PTFE substrate, with the inset showing a high-resolution image of a single nanocone. The periodicity of the nanocones is 1 μm. A 70-nm-thick Au layer was then sputtered over these cone arrays using an AJA International, Inc./Orion Sputter PHASE. The sputtering parameters used were 50 W power, 7.4×10^{-7} torr chamber vacuum, and a deposition rate of 6 nm/min. A chemical vapor deposition (CVD) grown WSe_2 monolayer was transferred

over the as-fabricated cone array using a poly(methyl methacrylate) (PMMA-)assisted wet transfer method [23].

B. Monolayer TMDC growth and integration

We optimized the CVD process to obtain large-area growth of the monolayer of around centimeter scale. The optical microscopy image of the as-grown WSe_2 monolayers is shown in Fig. 1(c). Raman spectra with characteristic E^1_{2g} peak at 249.82 cm^{-1} and the absence of B_{2g} peak at 303 cm^{-1} and PL spectra with emission peak at 1.67 eV in Figs. 1(d) and 1(e) confirm the presence of the monolayer [24,25]. This CVD-grown WSe_2 monolayer was then transferred over SiO_2 substrate using the PMMA-assisted wet transfer method as demonstrated in Fig. 1(f) over both the PTFE cone and Au-coated PTFE cones. The wet transfer method relies on weakening the interaction of the 2D material with the substrate by using solutions such as water [26] or NaOH/KOH [23], whereas the strong interaction of the 2D material with the top coated polymer (PMMA in our case) remains unaffected by these solutions. The SEM image in Fig. 1(g) shows the as-transferred monolayer over the cone array. These monolayers form a tent-like structure due to the tip of the cone, as shown in the inset of Fig. 1(g).

C. FDTD simulation

To simulate the excitonic emission in a WSe_2 monolayer integrated with the Au and PTFE nanocone array, the FDTD numerical method (using Ansys/Lumerical commercial simulation software) was employed. In the simulation setup, the system is enclosed inside a $1000 \times 1000 \times 4500$ nm^3 FDTD boundary. The mesh size of the whole simulation was fixed to 2 nm. PL enhancement consists of two factors, excitation enhancement and emission enhancement factor. Excitation enhancement is calculated as the ratio of electric field intensity in the presence and absence of the plasmonic nanocone, given by $F = |E|^2/|E_o|^2$, where $|E|$ and $|E_o|$ are the electric field magnitudes with and without the plasmonic structure. For emission enhancement, the exciton in the monolayer was simulated as a horizontal dipole source, sitting 5 nm on the top of the cone surface. Emission enhancement is calculated using [27]

$$Q = \frac{P_{\text{rad}}}{(P_{\text{tot}} + (1-\eta)P^o_{\text{rad}}/\eta)}. \quad (1)$$

Here P_{rad} is the far-field radiated power, which is collected over the numerical aperture (NA) of the microscope (NA = 0.4) in the presence of the nanocone structures, P_{tot} and P^o_{rad} are the total power radiated by the dipole with and without the structure, respectively, and η corresponds to the intrinsic PL quantum yield of the WSe_2, taken with a typical range of values from the literature [28–30] as 0.001, 0.01, 0.015, and 0.03.

For our system, we draw a comparison between PL enhancement factors obtained for only PTFE and Au-covered PTFE cones to explain the experimental results.

D. Optical characterisation

Raman spectroscopy was used to confirm the presence of WSe_2 monolayers. Raman spectra for the as-fabricated samples were recorded using an HR800-UV confocal micro-Raman spectrometer with the help of a 100× objective with an excitation source of 532 nm laser light having 1.1 mW power. The Raman spectrometer was initially calibrated with the standard Raman peak of crystalline silicon at 520.7 cm^{-1}. The acquisition time for Raman scattered light collection was 20 s. PL measurements were carried out by using a custom-made PL setup using a 532 nm excitation source, collected with a 20× Mitutoyo Plan Apo NIR Infinity Corrected Objective. Spectra were recorded using a Kymera 328i Andor spectrometer.

III. RESULTS AND DISCUSSION

We measured the emission from monolayer TMDC integrated with both PTFE and Au-coated PTFE nanocone arrays to understand the difference between TMDC interaction with plasmonic and dielectric antennae platforms. The standard PL spectrum of the WSe_2-coated PTFE and Au cones recorded with a 532 nm laser excitation in Fig. 2(a) shows about eight to ten times enhancement in the PL intensity with Au coating. We attribute this enhancement in PL emission of the monolayer WSe_2 in the case of Au-coated cones to the plasmonic properties of Au. We found that this enhancement is strongly dependent on the excitation power, hence we performed systematic PL measurements with varying laser fluences for the two cases. Figures 2(b) and 2(c) clearly shows higher PL intensity for Au-coated cones at all excitation powers. The color map of the ratio of PL intensity of the two cases (Au-coated/PTFE) is presented in Fig. 2(d), which shows an eight to ten times enhancement for low fluence to high fluence, respectively, for Au-coated cones as compared with the dielectric PTFE cones (inset shows the line plot where the PL enhancement is approximately eight to ten times).

A. Plasmonic enhancement

If the plasmon resonance of the plasmonic-TMDC system matches with the excitation frequency, the excitation rate of the TMDC will be enhanced. Further, a plasmon resonance at the particular PL frequency can enhance the emission rate [31–33]. This means that the PL enhancement in the plasmonic-TMDC system contains two terms, which are the excitation and emission enhancement [27]. We calculated both excitation and emission enhancement [27] using Lumerical FDTD simulation (see the Methods section) for both types of nanocones. In Figs. 2(e)

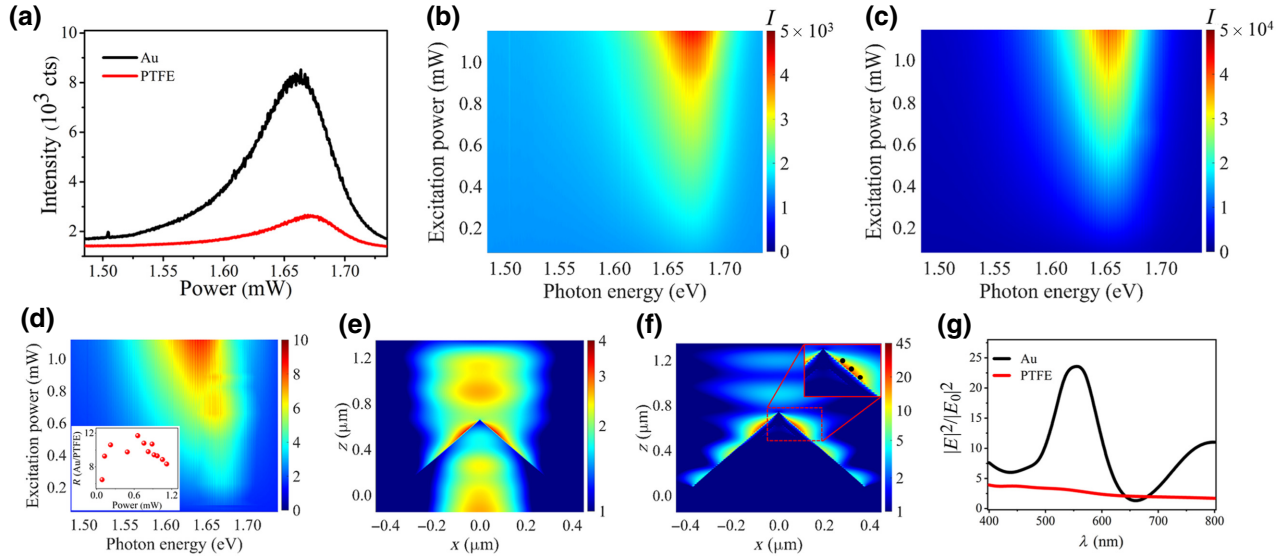

FIG. 2. PL enhancement at various excitation powers and the explanation with FDTD simulation. (a) Micro-PL spectra of the transferred WSe_2 over PTFE and Au nanocone structures. (b)–(d) PL intensity with the variation of the excitation energy for (b) PTFE cones, (c) Au cones, and (d) ratio (R) between Au and PTFE (inset shows the line plot for ratio R for maximum of the PL peak intensity (Au/PTFE) with the excitation power). (e), (f) FDTD simulation for the calculation of field enhancement for (e) PTFE cone and (f) Au cone. (g) Line spectra for the electric field enhancement showing resonance.

and 2(f), the excitation enhancements for the PTFE and Au cones are shown. Here the periodicity for the nanocone is 1 μm because it is resonant with the excitation wavelength, whereas 0.8 μm and 1.2 μm, which are not resonant at 532 nm, are shown in Fig. 1 within the Supplemental Material [34]. A clear enhancement of more than ten times for positions close to the cone tip can be observed for the Au cone as compared with the dielectric cone.

We further calculated emission enhancement for a dipole placed in close proximity of the tip, that is, at $x = 70$, 80, and 90 nm, denoted by black dots in the inset of the Fig. 2(f), as discussed in the Methods section. For the further confirmation of the plasmonic resonance at the excitation wavelength and emission wavelength, the absolute square of the electric field at $x = 70$ nm is plotted for both PTFE and Au cones in Fig. 2(g). In the PTFE cone case there is no resonance seen, whereas in the Au case there is about 20 times electric field intensity enhancement at the excitation wavelength and around ten times at emission wavelength. If we account for the internal quantum yield, these simulations show that, for positions close to the cone tip, an enhancement of ≈ 3 to ≈ 6.5 times can be observed for different values of quantum yield in an Au-coated cone as compared with the PTFE cone (see Table I, which is in the same range as the experimentally measured PL enhancement.

TABLE I. Theoretically calculated PL enhancement ratios (Au/PTFE) at positions $x = 70$, 80, and 90 nm for different values of η.

x (nm)	$\eta = 0.001$	$\eta = 0.01$	$\eta = 0.015$	$\eta = 0.03$
70	4.96	5.06	3.84	3.1
80	5.82	4.5	4	3.01
90	6.57	4.19	4.49	3.3

B. Excitation-dependent PL enhancement

To explain the nonlinear PL enhancement as discussed here, we fitted the PL spectra for the PTFE and Au cases with a double Lorentzian as shown in Figs. 3(a) and 3(b), respectively. This provides information about the relative exciton and trion contributions and their role in the PL enhancement. We plotted the integrated PL intensity for the exciton and trion as a function of excitation fluence for both samples and observed a linear relation as shown in Fig. 3(c). The slopes for the Au cones for exciton and trion intensities are found to be 1.03 and 1.07, respectively, whereas for the PTFE cones they were 0.97 and 0.95, respectively. This suggests that we are in a linear regime where the excitation power and the exciton and trion intensities are proportional. At higher excitation powers, we might encounter exciton-exciton interactions, which can result in a sublinear dependence [35].

We further plotted the intensity spectral weight $I_m/(I_E + I_T)$ for excitons and trions in Fig. 3(d), where subscript E represents exciton, T represents trion, and m denotes either E or T. This quantity provides information about the electrostatic charge neutrality of the monolayer. We can see that the spectral weight for the excitons in Au and PTFE is approximately 60% and 55%, respectively, whereas the

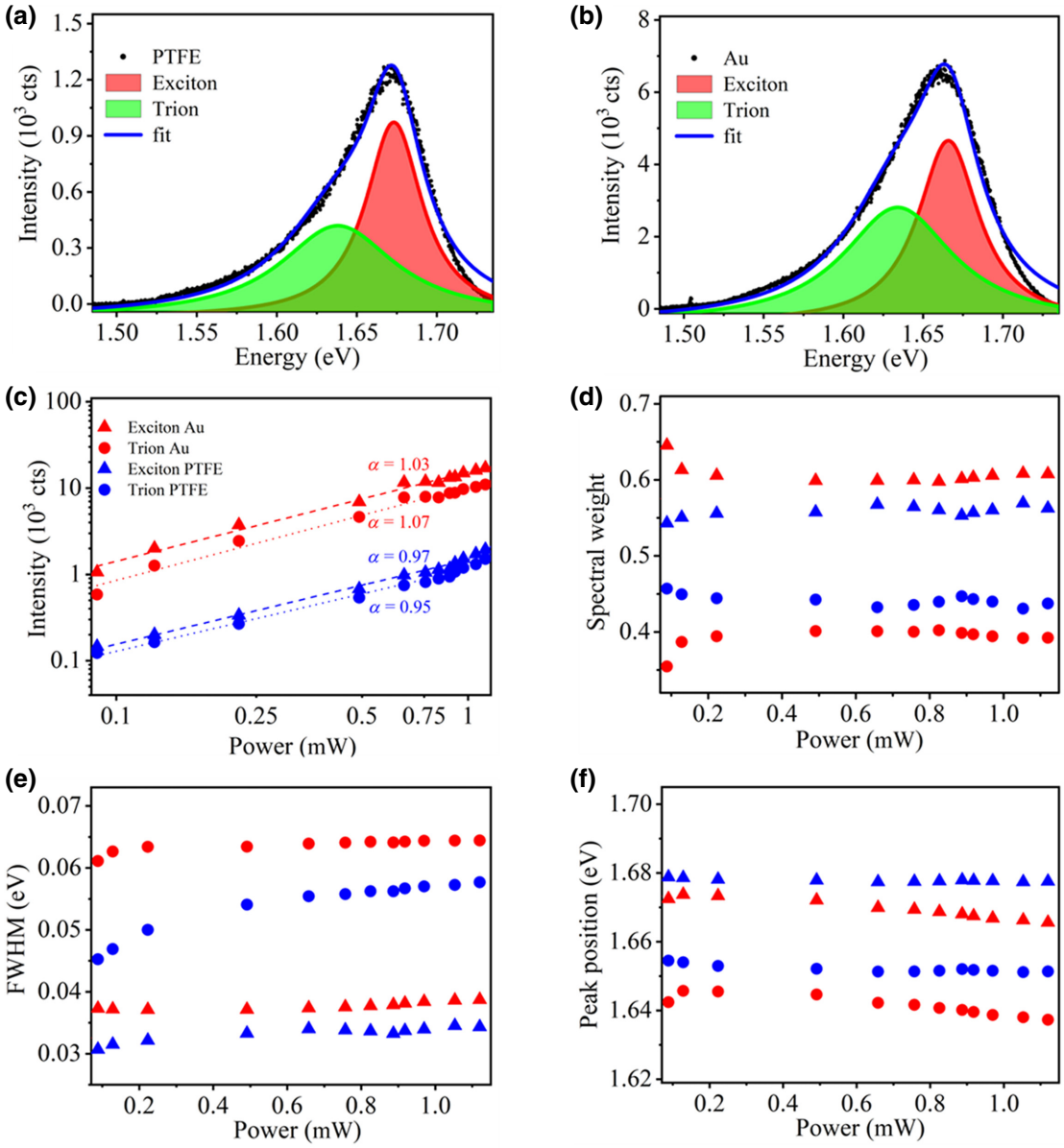

FIG. 3. Exciton-trion characteristics with excitation power after fitting with double Lorentzian. (a), (b) PL spectra at the 532 nm pump laser fitted with double Lorentzian for (a) WSe_2 transferred over PTFE cone and (b) WSe_2 transferred over Au cone. (c) PL intensity at various excitation energies with linear fitting (α denotes the slope), (d) intensity spectral weight for the exciton and trion, (e) FWHM of the exciton and trion, and (f) peak position for the exciton and trion, in PTFE and Au cones.

trion spectral weight in Au and PTFE is approximately 40% and 45%, respectively. It is known that the trion recombination pathway is mostly nonradiative [36]. From here, it is clear that the population of excitons is increasing, whereas trions are decreasing in the case of the Au. This increased population of the excitons in Au-coated cones can also contribute to the PL enhancement as compared with the bare PTFE cones [37]. PL enhancement has previously been reported due to substrate-dependent changes [38,39] and hot electron doping [40]. In our case, from the calculated local fields shown in Figs. 2(e) and 2(f), there is an order-of-magnitude enhancement in cones deposited with Au compared with those without Au coating.

Next we measured the features of the exciton and trion peaks, full width at half maxima (FWHM) and peak positions with increasing excitation powers. As shown in Fig. 3(e), the FWHM for both these cases increases slightly with increase in excitation power. This can be attributed to an increased dephasing of these excitons and trions due to interaction with the increasing background of free carriers. Further, the increased FWHM can also occur due to heating of the samples due to laser irradiation, which

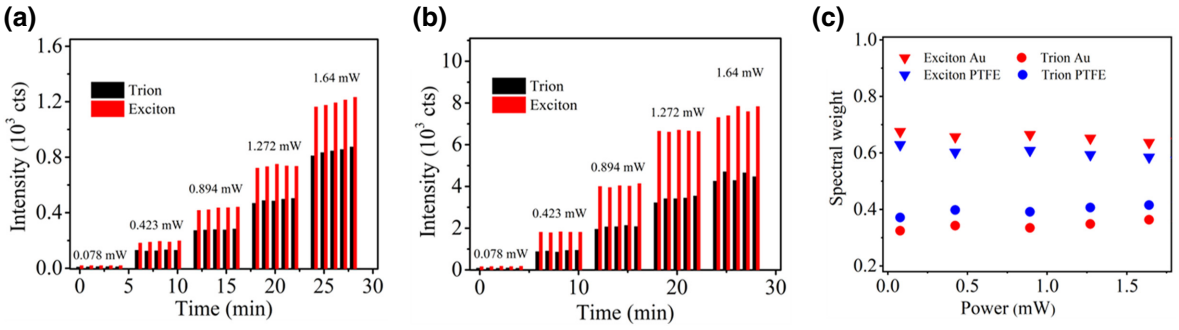

FIG. 4. Time-dependent analysis for the exciton-trion characteristics. Intensity of the integrated peak as a function of time for (a) PTFE and (b) Au. (c) The variation of intensity spectral weight with excitation power.

causes an increased phonon excitation and the exciton-phonon coupling results in broadening of the spectra [41, 42]. This photoinduced heating effect is more dominant for the plasmonic case versus nonplasmonic, as reported elsewhere [43]. Next, we observe a small redshift in the exciton and trion peak positions with increasing excitation power. Usually, the band-gap renormalization effect and carrier-screening-induced exciton-binding-energy lowering change oppositely with increased excitation power [44,45]. However, because we observe only the redshift of the peak, the former effect dominates in our case. However, in our range of powers, these shifts are small compared with the respective peak positions, hence should not impact the performance of nanophotonic devices built using our platform.

Next we measured the time evolution of the excitonic and trionic features by recording PL for several minutes at fixed values of pump power. We plot the intensity of the integrated PL peak as a function of time and the excitation power in Fig. 4. For both PTFE and Au cones, the intensity did not change much with the time [see Figs. 4(a) and 4(b)]. We also plotted the intensity spectral weight for the fourth minute and observed that the excitonic spectral weight has the same trend as that observed previously in Fig. 3(d), hence confirming the stability of our system with time.

IV. CONCLUSION

In summary, we have presented the integration of 2D TMDCs with a low-cost and large-area plasmonic nanocone array platform. We studied the exciton characteristics and resulting PL enhancement when the nanocones are covered with a plasmonic material. We observed a PL enhancement of eight to ten times, which was explained using FDTD simulations and higher excitonic spectral weight. Other than the traditional avenues of plasmon-enhanced optoelectronics [13], our platform would enable unique applications to deterministic strain [46] and dielectric-screening-based periodic modulation of the optical response of 2D semiconductors [47,48], including the development of quantum emitter arrays [49,50], exciton-funneling-based devices [51–54], and the observation of dark excitons [55–57]. The purpose of choosing WSe_2 is to study the dark excitonic states in tungsten-based TMDCs [58].

ACKNOWLEDGMENTS

A.K.S. acknowledges financial support from Industrial Research and Consultancy Center (IRCC), IIT Bombay. A.K. acknowledges funding support from the Department of Science and Technology via the grants: SB/S2/RJN-110/2017, ECR/2018/001485, and DST/NM/NS-2018/49. We acknowledge the Centre of Excellence in Nanoelectronics (CEN) at IIT Bombay for providing fabrication facilities.

[1] S. Manzeli, D. Ovchinnikov, D. Pasquier, O. V. Yazyev, and A. Kis, 2D transition metal dichalcogenides, Nat. Rev. Mater. **2**, 17033 (2017).

[2] K. F. Mak, C. Lee, J. Hone, J. Shan, and T. F. Heinz, Atomically Thin MoS_2: A New Direct-Gap Semiconductor, Phys. Rev. Lett. **105**, 136805 (2010).

[3] A. Ramasubramaniam, Large excitonic effects in monolayers of molybdenum and tungsten dichalcogenides, Phys. Rev. B **86**, 115409 (2012).

[4] A. Kormányos, G. Burkard, M. Gmitra, J. Fabian, V. Zólyomi, N. D. Drummond, and V. Fal'ko, $\mathbf{k}\cdot\mathbf{p}$ theory for two-dimensional transition metal dichalcogenide semiconductors, 2D Mater. **2**, 022001 (2015).

[5] K. F. Mak and J. Shan, Photonics and optoelectronics of 2D semiconductor transition metal dichalcogenides, Nat. Photonics **10**, 216 (2016).

[6] A. Pospischil and T. Mueller, Optoelectronic devices based on atomically thin transition metal dichalcogenides, Appl. Sci. **6**, 78 (2016).

[7] E. Lee, Y. S. Yoon, and D.-J. Kim, Two-dimensional transition metal dichalcogenides and metal oxide hybrids for gas sensing, ACS Sens. **3**, 2045 (2018).

[8] L. Wang, L. Huang, W. C. Tan, X. Feng, L. Chen, X. Huang, and K.-W. Ang, 2D photovoltaic devices: Progress and prospects, Small Methods **2**, 1700294 (2018).

[9] X. Liu and M. C. Hersam, 2D materials for quantum information science, Nat. Rev. Mater. **4**, 669 (2019).

[10] D. Xiao, G.-B. Liu, W. Feng, X. Xu, and W. Yao, Coupled Spin and Valley Physics in Monolayers of MoS_2 and Other Group-VI Dichalcogenides, Phys. Rev. Lett. **108**, 196802 (2012).

[11] C. Schneider, M. M. Glazov, T. Korn, S. Höfling, and B. Urbaszek, Two-dimensional semiconductors in the regime of strong light-matter coupling, Nat. Commun. **9**, 2695 (2018).

[12] A. Krasnok, S. Lepeshov, and A. Alú, Nanophotonics with 2D transition metal dichalcogenides [invited], Opt. Express **26**, 15972 (2018).

[13] S. Yan, X. Zhu, J. Dong, Y. Ding, and S. Xiao, 2D materials integrated with metallic nanostructures: Fundamentals and optoelectronic applications, Nanophotonics **9**, 1877 (2020).

[14] X. Li, J. Zhu, and B. Wei, Hybrid nanostructures of metal/two-dimensional nanomaterials for plasmon-enhanced applications, Chem. Soc. Rev. **45**, 3145 (2016).

[15] X. Li, J. Zhu, and B. Wei, Hybrid nanostructures of metal/two-dimensional nanomaterials for plasmon-enhanced applications, Chem. Soc. Rev. **45**, 3145 (2016).

[16] J. You, Y. Luo, J. Yang, J. Zhang, K. Yin, K. Wei, X. Zheng, and T. Jiang, Hybrid/integrated silicon photonics based on 2D materials in optical communication nanosystems, Laser Photonics Rev. **14**, 2000239 (2020).

[17] A. Castellanos-Gomez, Why all the fuss about 2D semiconductors?, Nat. Photonics **10**, 202 (2016).

[18] S. Kasani, K. Curtin, and N. Wu, A review of 2D and 3D plasmonic nanostructure array patterns: Fabrication, light management and sensing applications, Nanophotonics **8**, 2065 (2019).

[19] G. Zhang and D. Wang, Colloidal lithography-the art of nanochemical patterning, Chem. Asian J. **4**, 236 (2009).

[20] A. K. Singh, K. K. Mandal, A. A. VS, A. Kumar, S. Dixit, and A. Kumar, in *Nanoengineering: Fabrication, Properties, Optics, Thin Films, and Devices XVIII*, edited by W. Park, A.-J. Attias, and B. Panchapakesan (SPIE, San Diego, California, United States, 2021).

[21] J. Sun, C. J. Tang, P. Zhan, Z. L. Han, Z.-S. Cao, and Z.-L. Wang, Fabrication of centimeter-sized single-domain two-dimensional colloidal crystals in a wedge-shaped cell under capillary forces, Langmuir **26**, 7859 (2010).

[22] B. G. Prevo and O. D. Velev, Controlled, rapid deposition of structured coatings from micro- and nanoparticle suspensions, Langmuir **20**, 2099 (2004).

[23] H. Li, A. W. Contryman, X. Qian, S. M. Ardakani, Y. Gong, X. Wang, J. M. Weisse, C. H. Lee, J. Zhao, P. M. Ajayan, J. Li, H. C. Manoharan, and X. Zheng, Optoelectronic crystal of artificial atoms in strain-textured molybdenum disulphide, Nat. Commun. **6**, 7381 (2015).

[24] Q. Feng, M. Zhu, Y. Zhao, H. Liu, M. Li, J. Zheng, H. Xu, and Y. Jiang, Chemical vapor deposition growth of sub-centimeter single crystal WSe_2 monolayer by NaCl-assistant, Nanotechnology **30**, 034001 (2018).

[25] B. Liu, M. Fathi, L. Chen, A. Abbas, Y. Ma, and C. Zhou, Chemical vapor deposition growth of monolayer WSe_2 with tunable device characteristics and growth mechanism study, ACS Nano **9**, 6119 (2015).

[26] F. Zhang, C. Erb, L. Runkle, X. Zhang, and N. Alem, Etchant-free transfer of 2D nanostructures, Nanotechnology **29**, 025602 (2017).

[27] P. Bharadwaj and L. Novotny, Spectral dependence of single molecule fluorescence enhancement, Opt. Express **15**, 14266 (2007).

[28] M. S. Eggleston, S. B. Desai, K. Messer, S. A. Fortuna, S. Madhvapathy, J. Xiao, X. Zhang, E. Yablonovitch, A. Javey, M. C. Wu, *et al.*, Ultrafast spontaneous emission from a slot-antenna coupled WSe_2 monolayer, ACS Photonics **5**, 2701 (2018).

[29] H. Kim, G. H. Ahn, J. Cho, M. Amani, J. P. Mastandrea, C. K. Groschner, D.-H. Lien, Y. Zhao, J. W. Ager, M. C. Scott, D. C. Chrzan, and A. Javey, Synthetic WSe_2 monolayers with high photoluminescence quantum yield, Sci. Adv. **5**, eaau4728 (2019).

[30] C. Javerzac-Galy, A. Kumar, R. D. Schilling, N. Piro, S. Khorasani, M. Barbone, I. Goykhman, J. B. Khurgin, A. C. Ferrari, T. J. Kippenberg, *et al.*, Excitonic emission of monolayer semiconductors near-field coupled to high-q microresonators, Nano Lett. **18**, 3138 (2018).

[31] P. M. Marcus, Proceedings of the American Physical Society, Phys. Rev. **69**, 674 (1946).

[32] Z. Wang, Z. Dong, Y. Gu, Y.-H. Chang, L. Zhang, L.-J. Li, W. Zhao, G. Eda, W. Zhang, G. Grinblat, S. A. Maier, J. K. W. Yang, C.-W. Qiu, and A. T. S. Wee, Giant photoluminescence enhancement in tungsten-diselenide–gold plasmonic hybrid structures, Nat. Commun. **7**, 11283 (2016).

[33] O. Salehzadeh, M. Djavid, N. H. Tran, I. Shih, and Z. Mi, Optically pumped two-dimensional MoS2 lasers operating at room-temperature, Nano Lett. **15**, 5302 (2015).

[34] See Supplemental Material at http://link.aps.org/supplemental/10.1103/PhysRevApplied.19.044012 for the optimization of bead size, distinction of exciton versus trion contributions and discussion on tungsten versus molybdenum TMDCs.

[35] A. O. A. Tanoh, J. Alexander-Webber, J. Xiao, G. Delport, C. A. Williams, H. Bretscher, N. Gauriot, J. Allardice, R. Pandya, Y. Fan, Z. Li, S. Vignolini, S. D. Stranks, S. Hofmann, and A. Rao, Enhancing photoluminescence and mobilities in WS_2 monolayers with oleic acid ligands, Nano Lett. **19**, 6299 (2019).

[36] D.-H. Lien, S. Z. Uddin, M. Yeh, M. Amani, H. Kim, J. W. Ager, E. Yablonovitch, and A. Javey, Electrical suppression of all nonradiative recombination pathways in monolayer semiconductors, Science **364**, 468 (2019).

[37] Y. Tao, X. Yu, J. Li, H. Liang, Y. Zhang, W. Huang, and Q. J. Wang, Bright monolayer tungsten disulfide via exciton and trion chemical modulations, Nanoscale **10**, 6294 (2018).

[38] M. Buscema, G. A. Steele, H. S. J. van der Zant, and A. Castellanos-Gomez, The effect of the substrate on the Raman and photoluminescence emission of single-layer MoS_2, Nano Res. **7**, 561 (2014).

[39] H. Kwon, Substrate dependence of charged exciton (trion) for single-layer molybdenum disulfide, Bull. Korean Chem. Soc. **39**, 1176 (2018).

[40] X. Wen, W. Wang, X. Zhang, H. Chen, S. Jia, Y. Gong, W. Chen, Y. Wang, H. Zhu, J. Zheng, P. M. Ajayan, and J.

Lou, Pathways of exciton triggered hot-carrier injection at plasmonic metal-transition metal dichalcogenide interface, Adv. Opt. Mater. **10**, 2100070 (2022).

[41] N. Lundt, E. Cherotchenko, O. Iff, X. Fan, Y. Shen, P. Bigenwald, A. V. Kavokin, S. Höfling, and C. Schneider, The interplay between excitons and trions in a monolayer of $MoSe_2$, Appl. Phys. Lett. **112**, 031107 (2018).

[42] R. Kaupmees, P. Walke, L. Madauß, A. Maas, E. Pollmann, M. Schleberger, M. Grossberg, and J. Krustok, The effect of elevated temperatures on excitonic emission and degradation processes of WS_2 monolayers, Phys. Chem. Chem. Phys. **22**, 22609 (2020).

[43] S. Najmaei, A. Mlayah, A. Arbouet, C. Girard, J. Léotin, and J. Lou, Plasmonic pumping of excitonic photoluminescence in hybrid MoS_2–Au nanostructures, ACS Nano **8**, 12682 (2014).

[44] Y. Park, S. W. Han, C. C. S. Chan, B. P. L. Reid, R. A. Taylor, N. Kim, Y. Jo, H. Im, and K. S. Kim, Interplay between many body effects and coulomb screening in the optical bandgap of atomically thin MoS_2, Nanoscale **9**, 10647 (2017).

[45] P. D. Cunningham, A. T. Hanbicki, K. M. McCreary, and B. T. Jonker, Photoinduced bandgap renormalization and exciton binding energy reduction in WS_2, ACS Nano **11**, 12601 (2017).

[46] B. Aslan, M. Deng, M. L. Brongersma, and T. F. Heinz, Strained bilayer WSe_2 with reduced exciton-phonon coupling, Phys. Rev. B **101**, 115305 (2020).

[47] Z. Peng, X. Chen, Y. Fan, D. J. Srolovitz, and D. Lei, Strain engineering of 2D semiconductors and graphene: From strain fields to band-structure tuning and photonic applications, Light: Sci. Appl. **9**, 190 (2020).

[48] B. Aslan, C. Yule, Y. Yu, Y. J. Lee, T. F. Heinz, L. Cao, and M. L. Brongersma, Excitons in strained and suspended monolayer WSe_2, 2D Mater. **9**, 015002 (2021).

[49] C. Chakraborty, N. Vamivakas, and D. Englund, Advances in quantum light emission from 2D materials, Nanophotonics **8**, 2017 (2019).

[50] L. Yu, M. Deng, J. L. Zhang, S. Borghardt, B. Kardynal, J. Vučković, and T. F. Heinz, Site-controlled quantum emitters in monolayer $MoSe_2$, Nano Lett. **21**, 2376 (2021).

[51] J. Feng, X. Qian, C.-W. Huang, and J. Li, Strain-engineered artificial atom as a broad-spectrum solar energy funnel, Nat. Photonics **6**, 866 (2012).

[52] H. Moon, G. Grosso, C. Chakraborty, C. Peng, T. Taniguchi, K. Watanabe, and D. Englund, Dynamic exciton funneling by local strain control in a monolayer semiconductor, Nano Lett. **20**, 6791 (2020).

[53] J. Lee, S. J. Yun, C. Seo, K. Cho, T. S. Kim, G. H. An, K. Kang, H. S. Lee, and J. Kim, Switchable, tunable, and directable exciton funneling in periodically wrinkled WS_2, Nano Lett. **21**, 43 (2020).

[54] H. Su, D. Xu, S.-W. Cheng, B. Li, S. Liu, K. Watanabe, T. Taniguchi, T. C. Berkelbach, J. C. Hone, M. Delor, *et al.*, Dark-exciton driven energy funneling into dielectric inhomogeneities in two-dimensional semiconductors, Nano Lett. **22**, 2843 (2022).

[55] S. B. Chand, J. M. Woods, E. Mejia, T. Taniguchi, K. Watanabe, and G. Grosso, Visualization of dark excitons in semiconductor monolayers for high-sensitivity strain sensing, Nano Lett. **22**, 3087 (2022).

[56] M. Rahaman, O. Selyshchev, Y. Pan, R. Schwartz, I. Milekhin, A. Sharma, G. Salvan, S. Gemming, T. Korn, D. R. T. Zahn, *et al.*, Observation of room-temperature dark exciton emission in nanopatch-decorated monolayer WSe_2 on metal substrate, Adv. Opt. Mater. **9**, 2101801 (2021).

[57] G. Wang, C. Robert, A. Suslu, B. Chen, S. Yang, S. Alamdari, I. C. Gerber, T. Amand, X. Marie, S. Tongay, and B. Urbaszek, Spin-orbit engineering in transition metal dichalcogenide alloy monolayers, Nat. Commun. **6**, 10110 (2015).

[58] E. Malic, M. Selig, M. Feierabend, S. Brem, D. Christiansen, F. Wendler, A. Knorr, and G. Berghäuser, Dark excitons in transition metal dichalcogenides, Phys. Rev. Mater. **2**, 014002 (2018).